

Computational Modeling of Cancer Response to Oncolytic Virotherapy: Improving the Effectiveness of Viral Spread and Anti Tumor Efficacy



H. Lefraich

1 Introduction

Oncolytic virotherapy represents a promising anti-cancer treatment approach, which involves viruses that have been selectively engineered to infect and destroy cancer cells, while sparing the surrounding healthy cells [1–4]. These oncolytic viruses can penetrate cancer cells either through receptor binding, or through fusion with plasma membrane, then they replicate by taking advantage of signaling pathways and common mutations inside those cancer cells. Despite the oncolytic viruses can enter also healthy cells, they do not usually replicate inside these cells and thus do not destroy them. In fact, the absence of such mutations in healthy cells tends to abort the replication cycle of the viruses. In 2015, the United States of America Food and Drug Administration (FDA), based on the recent advances in the understanding of tumor-virus interactions, approved the first genetically engineered OV (a Herpes Simplex Virus) as a therapy for the melanoma cancer [3]. However, despite the fact that multiple oncolytic viruses (OVs) are presently under clinical development [1, 5], this kind of therapy still has some challenges in terms of effectiveness (as confirmed by several clinical trials) [6]. This relatively low oncolytic effectiveness is not only due to premature virus clearance by circulating antibodies and various immune cells [7], but also the presence of physical barriers inside tumors (e.g., interstitial fluid pressure, extracellular matrix (ECM) deposits) that hinder virus movement [8]. In fact, the ECM has been recognized as a major barrier for anti-tumor efficacy as it plays a pivotal role in inhibiting virus spread [9–11]. To face the challenge of improving the intra-tumoral spread of oncolytic viruses, numerous experimental and clinical approaches are currently being considered,

H. Lefraich (✉)

Laboratory (MISI), Faculty of Sciences and techniques, Department of Mathematics and Computer Science, University Hassan First, Settat, Morocco

from genetically manipulating natural OV's to incorporate additional features for improving their efficiency [5], to modifications of the physical barriers (e.g., via ECM degradation) to improve virus spread [11]. Understanding more deeply the interactions between the extracellular matrix (ECM), uninfected and infected cancer cells, and oncolytic viruses is therefore of great importance to shed a light on the biological mechanisms that might improve OV spread by overcoming the physical barriers inside the tumor micro-environment.

During the last two decades, numerous mathematical models have been applied to gaining a broader understanding of the dynamics of virotherapy by analyzing more deeply the interaction between cancer cells and oncolytic viruses. Concerning ordinary differential equations models, one can refer to Wodarz in [12–14], Komarova and Wodarz [15], Novozhilov et al. [16], Bajzer et al. [17, 18], Tian in [19, 20] and others [21–24]. Wodarz [13] formulated a simple model with two differential equations where a virus is interacting with a population of uninfected and virus-infected tumour cells. Based on this work, Komarova and Wodarz [15] used a general approach by taking into account a class of models instead of a specific model and considered two populations: uninfected tumour cells and infected tumour cells. Wodarz in his paper [14] proposed a model with three populations where he modeled explicitly the viral population. Then, Tian [20] has proposed an improved model by incorporating the burst size. The burst size of a virus is the number of new virions released from a lysis of an infected cell. The model is given by

$$\begin{cases} \frac{dc}{dt} = \mu_1 c \left(1 - \frac{c+i}{C}\right) - \rho cv \\ \frac{di}{dt} = \rho cv - \delta_i i \\ \frac{dv}{dt} = b\delta_i i - \rho cv - \delta_v v \end{cases}$$

The populations of the model consist of the densities within three groups: uninfected cancer cells $c(t)$, infected cancer cells $i(t)$, and free virus $v(t)$. The constant C stands for the maximal tumor size. The term $\mu_1 c$ models the rate of growth of cancer cells, ρcv the rate of infection of cancer cells by the virus, $b\delta_i i$ the release of virions by infected cancer cells, $\delta_i i$ the rate of clearance of infected cancer cells, and $\delta_v v$ the rate of clearance of the virus. Besides, Novozhilov et al. [16] analyzed ratio based oncolytic virus infection models. Bajzer et al. [17] modeled the specific cancer virotherapy with measles virus by using three ordinary differential equations, and then they approached the optimization of viral doses, number of doses and timing in [18].

Because of the availability of temporal data the majority of these models approached the oncolytic viruses from temporal dynamics perspective. However, the main cause of mortality among cancer patients is the spread of primary

cancer cells to other parts of the body to establish secondary tumours (metastasis). Moreover, the diffusion of oncolytic viruses within the tumor can play a major role in the efficacy and success of the treatment [25, 26]. Consequently, the spatial dependency of the virotherapy needs also to be considered in mathematical models in order to realistically simulate the clinical observations. This shortcoming of ODE models necessitates the use of PDEs in the field of computational cancer biology. More recent advances in tumour imaging provided data on the spatial spread of tumours and viruses, which then encouraged the emergence of mathematical models investigating the spatial spread of these viruses. Thus, many partial differential equation models have been formulated to include both the spatial and temporal distributions of viruses and cells [27–32]. For instance, Wu et al. [27] and Wein et al. [28] proposed and analyzed a system of partial differential equations in order to describe some aspect of oncolytic viral therapy. Camara et al. [29] explored an important interaction between aggressively invasive glioma cancer cells and the free oncolytic virus “ONYX-015”. Malinzi et al. [30] developed a reaction-diffusion system and considered the impact of virotherapy on the concentration of the tumor cells in the presence of CTL immune response. Then, Malinzi et al. [32] proposed a PDE based model that study the effect of the combination of oncolytic virotherapy with chemotherapy.

All suggested computational models have given valuable insights into oncolytic virotherapy dynamics. Nevertheless, there is a tremendous need to understand the dynamics of oncolytic virotherapy in the presence of extracellular matrix (ECM), particularly, to understand the complex interplay among cancer cells, oncolytic viruses and the extracellular matrix. In fact, tumour cells encounter a large amount of insoluble intact adhesive molecules of the extracellular matrix (ECM), which may promote their directed migration at different stages in the process of cancer invasion. A cell would migrate from a region of low concentration of relevant adhesive molecules towards a region with a higher concentration. This phenomenon is termed haptotaxis [33, 34]. Furthermore, the ECM is considered as a major barrier to virus motility by acting like a porous medium.

In this study, we are interested in a mathematical modeling and computational approach of oncolytic virotherapy which aims to help us improve our understanding of the physical barrier that inhibits the virus spread. Therefore, we propose a mathematical model of oncolytic virotherapy, that accounts for interaction between uninfected cancer cells, infected cancer cells, extracellular matrix (ECM) and oncolytic virus. Besides random motion, both uninfected and infected tumour cells migrate haptotactically towards higher ECM densities, moreover, in addition to degrading the static ECM upon contact the two cancer populations undergo an infection-induced transition mechanism conducted by virus particles which are released by infected cancer cells, and which attack the uninfected part of the tumor. One of the main contributions of this model consists in taking into account that the motility rate of virus particles is controlled by the population of ECM where lowering ECM leads to higher viral diffusion. Accordingly, we defined the diffusivity of tumour cells as a monotonically decreasing function of ECM density to model the obstruction of movement by the ECM.

This chapter is organized as follows. In Sect. 2, the mathematical model as well as its dimensionless form are presented. The variational formulation, the temporal discretization, and the finite element scheme of the nonlinear system are presented in Sect. 3. Finally, we present numerical experiments and summarize the observations of this study.

2 Mathematical Model

In this section, we present a two-dimensional mathematical model of oncolytic virotherapy. The model consists of four unknown variables namely the uninfected cancer cells density, the infected cancer cells density, the ECM density and the oncolytic virus particles density, which are denoted respectively by $c(x, t)$, $i(x, t)$, $u(x, t)$ and $v(x, t)$. We consider the system to hold on a bounded spatial domain $\Omega \subset \mathbb{R}^2$, representing a region of tissue. As the tumour cells depend on the closest blood vessel, we assume that the computational domain Ω is a disc with a centered hole inside representing the blood vessel (see Fig. 1). The boundary of the domain consists of two parts $\partial\Omega = \partial\Omega_1 \cup \partial\Omega_2$, where $\partial\Omega_1$ refers to the intern boundary delimited by the blood vessel wall, and $\partial\Omega_2$ refers to the extern boundary of Ω . Moreover, we estimate the radius of this region supported by the blood vessel to be $\frac{r_b}{\sqrt{BVF}}$, where BVF is the blood volume fraction [35, 36], and r_b is the radius of the blood vessel. Concerning the viruses, they attain the tumor through the blood vessel via $\partial\Omega_1$ and diffuse into it with no flux at $\partial\Omega_2$. Furthermore, viruses are provided continuously with a constant concentration v_b (for instance by using nanotechnology [37]). Guided by the in vitro experimental protocol in which invasion takes place within an isolated system, we consider zero-flux boundary conditions at the blood vessel wall $\partial\Omega_1$ and at the extern boundary of the disc for the uninfected cancer cells, the infected cancer cells, and also for the ECM.

Uninfected Cancer Cells $c(x, t)$ The underlying modeling assumptions are that in addition to random cell movement (with D_c as the random motility coefficient), uninfected cancer cells have a directed haptotactic movement towards higher ECM gradients (with η_c the haptotactic coefficient). Moreover, cancer cells apart from possibly proliferating logistically at rate μ_1 [38, 39], can decay due to virus infection at rate ρ . These hypotheses can be described by the following equation:

$$\frac{\partial c}{\partial t} = D_c \Delta c - \eta_c \nabla \cdot (c \nabla u) + \mu_1 c \left(1 - \frac{c}{C} - \frac{i}{C}\right) - \rho c v,$$

where C is the carrying capacity of the cancer cells and the extracellular matrix.

Infected Cancer Cells $i(x, t)$ Similarly, we assume that the infected cancer cells can move randomly (with D_i as the random motility coefficient) and can migrate towards higher ECM gradients (with η_i the haptotactic coefficient). As mentioned

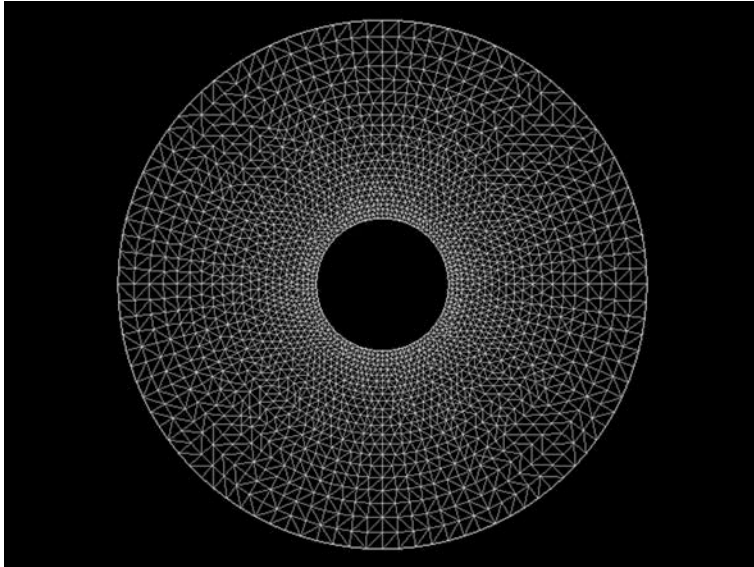


Fig. 1 Computational domain constructed. the computational domain Ω is a disc with a centered hole inside representing the blood vessel

above, these cells are infected at rate ρ by the oncolytic virus. Furthermore, these infected cells die owing to lysis at a rate δ_i . These assumptions are translated into the following equation:

$$\frac{\partial i}{\partial t} = D_i \Delta i - \eta_i \nabla \cdot (i \nabla u) + \rho cv - \delta_i i.$$

Extracellular Matrix (ECM) $u(x, t)$ The ECM can be regarded as static in the sense that it does not move, and thus we may neglect any diffusion and migration terms, however, it undergoes a continuous remodelling by cells in the environment [40]. We represent this remodeling process by the difference between a logistic growth term with rate μ_2 and a degradation term (where α_c is the rate of ECM degradation by uninfected cancer cells, and α_i is the rate of ECM degradation by infected cancer cells). Thus, the evolution of the ECM is governed by the following equation:

$$\frac{\partial u}{\partial t} = -u(\alpha_c c + \alpha_i i) + \mu_2 u \left(1 - \frac{u}{C} - \frac{c}{C} - \frac{i}{C}\right),$$

Oncolytic Virus $v(x, t)$ We assume that the virus can spread randomly in ECM density-dependent manner through the environment with $D_v(u)$ the random motility coefficient which quantifies how virus particles outside infected cells can freely move around less dense ECM. We opt for the phenomenological form:

$$D_v(u) = D_v(1 - \frac{u}{C}),$$

where D_v is a reference diffusion in absence of ECM. Furthermore, the virus particles duplicate at rate b , the burst size of infected cancer cells, which release the new virions in the environment. However, the number of free virus particles reduction is mainly due to the natural virion's death at rate δ_v , and the trapping of these virus particles into the cancer cells at rate ρ . In summary, the governing equation for the density of virus particles is as follows:

$$\frac{\partial v}{\partial t} = \nabla(D_v(u)\nabla v) + bi - \rho cv - \delta_v v.$$

In summary, we obtain the following system of PDE-ODE equations, where all the parameters in the system are nonnegative:

$$\left\{ \begin{array}{l} \frac{\partial c}{\partial t} = D_c \Delta c - \eta_c \nabla \cdot (c \nabla u) + \mu_1 c (1 - \frac{c}{C} - \frac{i}{C}) - \rho cv \quad \text{in } \Omega \times]0, T[, \\ \frac{\partial i}{\partial t} = D_i \Delta i - \eta_i \nabla \cdot (i \nabla u) + \rho cv - \delta_i i \quad \text{in } \Omega \times]0, T[, \\ \frac{\partial u}{\partial t} = -u(\alpha_c c + \alpha_i i) + \mu_2 u (1 - \frac{u}{C} - \frac{c}{C} - \frac{i}{C}) \quad \text{in } \Omega \times]0, T[, \\ \frac{\partial v}{\partial t} = \nabla(D_v(u)\nabla v) + bi - \rho cv - \delta_v v \quad \text{in } \Omega \times]0, T[. \end{array} \right. \tag{1}$$

Based on the aforementioned assumptions the system is closed with the following homogenous initial and boundary conditions:

$$\left\{ \begin{array}{l} c(x, 0) = c_0(x) \\ i(x, 0) = i_0(x) \\ u(x, 0) = u_0(x) \\ v(x, 0) = v_0(x) \end{array} \right.$$

$$\left\{ \begin{array}{l} D_c \frac{\partial c}{\partial n} + \eta_c c \frac{\partial u}{\partial n} = 0 \quad \text{in } \partial\Omega \times]0, T[, \\ D_i \frac{\partial i}{\partial n} + \eta_i i \frac{\partial u}{\partial n} = 0 \quad \text{in } \partial\Omega \times]0, T[, \\ D_v(u) \frac{\partial v}{\partial n} = 0 \quad \text{in } \partial\Omega_2 \times]0, T[, \\ v = v_b \quad \text{in } \partial\Omega_1 \times]0, T[, \end{array} \right.$$

where n is the outward normal vector to $\partial\Omega$ and v_b is the value of v at the blood vessel.

2.1 Dimensionless Form

Let $L = 0.1\text{cm}$ and $\tau = \frac{L^2}{D}$, (where $D \approx 10^{-6} \text{cm}^2 \text{s}^{-1}$ according to [41]) be the characteristic length and time scale respectively. We define the dimensionless variables as follows:

$$\tilde{c} = \frac{c}{C}, \quad \tilde{i} = \frac{i}{C}, \quad \tilde{u} = \frac{u}{C}, \quad \tilde{v} = \frac{v}{C}, \quad \tilde{x} = \frac{x}{L}, \quad \tilde{t} = \frac{t}{\tau}$$

and new parameters via the following scaling:

$$\tilde{D}_c = \frac{\tau D_c}{L^2}, \quad \tilde{D}_i = \frac{\tau D_i}{L^2}, \quad \tilde{D}_v = \frac{\tau D_v}{L^2}, \quad \tilde{\eta}_c = \eta_c \frac{\tau C}{L^2}, \quad \tilde{\eta}_i = \eta_i \frac{\tau C}{L^2}, \quad \tilde{\mu}_1 = \tau \mu_1,$$

$$\tilde{\rho} = \tau \rho C, \quad \tilde{\delta}_i = \tau \delta_i, \quad \tilde{\alpha}_c = \tau \alpha_c C, \quad \tilde{\alpha}_i = \tau \alpha_i C, \quad \tilde{\mu}_2 = \tau \mu_2, \quad \tilde{b} = \tau b, \quad \tilde{\delta}_v = \tau \delta_v$$

$$\widetilde{c(x, 0)} = \frac{c(x, 0)}{C}, \quad \widetilde{i(x, 0)} = \frac{i(x, 0)}{C}, \quad \widetilde{u(x, 0)} = \frac{u(x, 0)}{C}, \quad \widetilde{v(x, 0)} = \frac{v(x, 0)}{C}.$$

Henceforth, we drop the tilde over all variables for convenience. The dimensionless form of the model equations (1) can then be written in the following general form:

$$\left\{ \begin{array}{ll}
 \frac{\partial c}{\partial t} = D_c \Delta c - \eta_c \nabla \cdot (c \nabla u) + \mu_1 c(1 - c - i) - \rho c v & \text{in } \Omega \times]0, T[, \\
 \frac{\partial i}{\partial t} = D_i \Delta i - \eta_i \nabla \cdot (i \nabla u) + \rho c v - \delta_i i & \text{in } \Omega \times]0, T[, \\
 \frac{\partial u}{\partial t} = -u(\alpha_c c + \alpha_i i) + \mu_2 u(1 - u - c - i) & \text{in } \Omega \times]0, T[, \\
 \frac{\partial v}{\partial t} = \nabla \cdot (D_v(u) \nabla v) + b i - \rho c v - \delta_v v & \text{in } \Omega \times]0, T[, \\
 D_c \frac{\partial c}{\partial n} + \eta_c c \frac{\partial u}{\partial n} = 0 & \text{in } \partial \Omega \times]0, T[, \\
 D_i \frac{\partial i}{\partial n} + \eta_i i \frac{\partial u}{\partial n} = 0 & \text{in } \partial \Omega \times]0, T[, \\
 D_v(u) \frac{\partial v}{\partial n} = 0 & \text{in } \partial \Omega_2 \times]0, T[, \\
 v = v_b & \text{in } \partial \Omega_1 \times]0, T[, \\
 c(x, 0) = c_0(x) & \text{in } \Omega, \\
 i(x, 0) = i_0(x) & \text{in } \Omega, \\
 u(x, 0) = u_0(x) & \text{in } \Omega, \\
 v(x, 0) = v_0(x) & \text{in } \Omega.
 \end{array} \right. \tag{2}$$

We suppose that $c_0, i_0, u_0, v_0 \in L^2(\Omega)$ and are nonnegative.

3 Finite Element Scheme

The mathematical model (2) considered in the previous section is a highly nonlinear coupled system of partial and ordinary differential equations. Thus, we can't afford to solve it analytically. Aiming to solve it numerically, we present a finite element scheme in this section. First, we derive the variational formulation for the uninfected and infected cancer cells density equations, the ECM density equation and the virus density equation. Further, we present the temporal discretization of the model equations. Finally, we describe a fixed-point-iteration to handle the nonlinear terms in the system (2) and we provide an appropriate numerical scheme.

3.1 Variational Formulation

In order to show the numerical formulation of the problem, let $V = L^2(0, T; H^1(\Omega))$ be the space of approximate solutions and $W = H^1(\Omega)$ be the space of tests functions. Let W^h be a finite element space of Lagrange $P1$ included in W and $V^h = L^2(0, T; W^h)$ be the finite dimensional subspace of V . The Faedo-Galerkin formulation for the problem is given by, finding $c_h, i_h, u_h \in V$ and $v_h \in V$ such that $v_h = v_b^h$ in $\partial\Omega_1$:

$$\left\{ \begin{array}{l} \left(\frac{\partial c_h}{\partial t}, \phi \right) + a_c(c_h, c_h, i_h, u_h, v_h, \phi) = 0 \\ \left(\frac{\partial i_h}{\partial t}, \phi \right) + a_i(i_h, c_h, u_h, v_h, \phi) = 0 \\ \left(\frac{\partial u_h}{\partial t}, \phi \right) + a_u(u_h, u_h, c_h, i_h, \phi) = 0 \\ \left(\frac{\partial v_h}{\partial t}, \psi \right) + a_v(v_h, c_h, i_h, u_h, \psi) = 0 \\ c_h(x, 0) = c_{h,0}(x) \quad \text{in } \Omega, \\ i_h(x, 0) = i_{h,0}(x) \quad \text{in } \Omega, \\ u_h(x, 0) = u_{h,0}(x) \quad \text{in } \Omega, \\ v_h(x, 0) = v_{h,0}(x) \quad \text{in } \Omega, \end{array} \right. \quad (3)$$

for all $\phi \in W^h$ and $\psi \in W^h$ such that $\psi = 0$ in $\partial\Omega_1$, and a. e. $t \in]0, T[$ where:

$$a_c(c_1, c_2, i, u, v, \phi) = D_c \int_{\Omega} \nabla c_1 \cdot \nabla \phi dx - \eta_c \int_{\Omega} c_1 \nabla u \cdot \nabla \phi dx - \mu_1 \int_{\Omega} c_1(1 - c_2 - i) \phi dx + \rho \int_{\Omega} c_1 v \phi dx,$$

$$a_i(i, c, u, v, \phi) = D_i \int_{\Omega} \nabla i \cdot \nabla \phi dx - \eta_i \int_{\Omega} i \nabla u \cdot \nabla \phi dx - \rho \int_{\Omega} c v \phi dx + \delta_i \int_{\Omega} i \phi dx,$$

$$a_u(u_1, u_2, c, i, \phi) = \int_{\Omega} u_1(\alpha_c c + \alpha_i i) \phi dx - \mu_2 \int_{\Omega} u_1(1 - u_2 - c - i) \phi dx,$$

$$a_v(v, c, i, u, \psi) = \int_{\Omega} D_v(u) \nabla v \cdot \nabla \psi dx - b \int_{\Omega} i \psi dx + \rho \int_{\Omega} c v \psi dx + \delta_v \int_{\Omega} v \psi dx,$$

$c_{h,0}(x), i_{h,0}(x), u_{h,0}(x)$ and $v_{h,0}(x)$ are respectively the projections of $c_0(x), i_0(x), u_0(x)$ and $v_0(x)$ on W^h .

3.2 Discrete Problem

In this section, we present the temporal discretization of the coupled variational system (3), where we discussed the application of Crank-Nicolson time discretization.

3.2.1 Temporal Discretization

Let $0 = t^0 < t^1 < \dots < t^N = T$ be a decomposition of the considered time interval $]0, T[$, and $\delta_t = t^{n+1} - t^n$, $n = 0, 1, \dots, N - 1$ denotes the uniform time step. In addition, we use $c_h^n(x) := c_h(x, t^n)$, $i_h^n(x) := i_h(x, t^n)$, $u_h^n(x) := u_h(x, t^n)$ and $v_h^n(x) := v_h(x, t^n)$ to denote the approximation of the solutions at time t^n . We apply the implicit Crank-Nicolson discretization scheme, which is second order and A-stable, then the semi-discrete form of the system (3) reads:

For given c_h^{n-1} , i_h^{n-1} , u_h^{n-1} and v_h^{n-1} with $c_h^0 = c_{h,0}$, $i_h^0 = i_{h,0}$, $u_h^0 = u_{h,0}$ and $v_h^0 = v_{h,0}$, find $c_h^n, i_h^n, u_h^n \in W^h$ and $v_h^n \in W^h$ such that $v_h^n = v_b^n$ in $\partial\Omega_1$ such that:

$$\left\{ \begin{aligned} \left(\frac{c_h^n - c_h^{n-1}}{\delta_t}, \phi \right) + \frac{1}{2} a_c(c_h^n, c_h^n, i_h^n, u_h^n, v_h^n, \phi) &= -\frac{1}{2} a_c(c_h^{n-1}, c_h^{n-1}, i_h^{n-1}, u_h^{n-1}, v_h^{n-1}, \phi) \\ \left(\frac{i_h^n - i_h^{n-1}}{\delta_t}, \phi \right) + \frac{1}{2} a_i(i_h^n, c_h^n, u_h^n, v_h^n, \phi) &= -\frac{1}{2} a_i(i_h^{n-1}, c_h^{n-1}, u_h^{n-1}, v_h^{n-1}, \phi) \\ \left(\frac{u_h^n - u_h^{n-1}}{\delta_t}, \phi \right) + \frac{1}{2} a_u(u_h^n, u_h^n, c_h^n, i_h^n, \phi) &= -\frac{1}{2} a_u(u_h^{n-1}, u_h^{n-1}, c_h^{n-1}, i_h^{n-1}, \phi) \\ \left(\frac{v_h^n - v_h^{n-1}}{\delta_t}, \psi \right) + \frac{1}{2} a_v(v_h^n, c_h^n, i_h^n, u_h^n, \psi) &= -\frac{1}{2} a_v(v_h^{n-1}, c_h^{n-1}, i_h^{n-1}, u_h^{n-1}, \psi) \end{aligned} \right. \tag{4}$$

for all $\phi \in W^h$ and $\psi \in W^h$ such that $\psi = 0$ in $\partial\Omega_1$.

3.2.2 Numerical Scheme

The nonlinearity in the semi-discrete form of the system (4) besides the coupling between the equations makes the computations a very challenging task. In one hand, a fully implicit treatment of the nonlinear and coupled terms leads to a coupled nonlinear algebraic system and it will be a very tough task to solve it with a nonlinear solver, in the other hand an explicit treatment leads to a linearized system in which the equations are solved simultaneously. However, it may require a severe restriction on the time step. Accordingly, we suggest a fixed-point iteration method [42] to treat the nonlinear and coupled terms semi-implicitly. For instance, let us explain briefly the fixed point iteration steps for a nonlinear term in the uninfected cancer cells density equation in the time interval (t^{n-1}, t^n) . Let $c_{h,0}^n = c_h^{n-1}$, $u_{h,0}^n = u_h^{n-1}$ and $i_{h,0}^n = i_h^{n-1}$ and we replace the nonlinear integral terms in the uninfected cancer cells density with:

$$\int_{\Omega} c_{h,k}^n \nabla u_{h,k}^n \cdot \nabla \phi dx \simeq \int_{\Omega} c_{h,k}^n \nabla u_{h,k-1}^n \cdot \nabla \phi dx,$$

$$\int_{\Omega} c_{h,k}^n (1 - c_{h,k}^n - i_{h,k}^n) \phi dx \simeq \int_{\Omega} c_{h,k}^n (1 - c_{h,k-1}^n - i_{h,k-1}^n) \phi dx$$

for $k = 0, 1, 2, \dots$. We iterate until the residual of the system (4) is less than the prescribed threshold value (10^{-8}) or until the maximal number of iterations is reached. Finally, we set $c_h^n = c_{h,k}^n$ and advance to the next time step. We handle the nonlinear and coupled terms in all other equations in a similar way by using the above prescribed iteration of fixed point type. Consequently, the linearized form of the system (4) in the interval (t^{n-1}, t^n) reads:

For given $c_{h,0}^n = c_h^{n-1}$, $i_{h,0}^n = i_h^{n-1}$, $u_{h,0}^n = u_h^{n-1}$ and $v_{h,0}^n = v_h^{n-1}$ with $c_h^0 = c_{h,0}$, $i_h^0 = i_{h,0}$, $u_h^0 = u_{h,0}$ and $v_h^0 = v_{h,0}$, find $c_{h,k}^n$, $i_{h,k}^n$, $u_{h,k}^n$ and $v_{h,k}^n$ satisfying $v_{h,k}^n = v_b^h$ in $\partial\Omega_1$ such that for all $\phi \in W^h$ and $\psi \in W^h$ with $\psi = 0$ in $\partial\Omega_1$

$$\left\{ \begin{array}{l} (c_{h,k}^n, \phi) + \frac{\delta_t}{2} a_c(c_{h,k}^n, c_{h,k-1}^n, i_{h,k-1}^n, u_{h,k-1}^n, v_{h,k-1}^n, \phi) = (c_h^{n-1}, \phi) - \frac{\delta_t}{2} a_c(c_h^{n-1}, c_h^{n-1}, i_h^{n-1}, u_h^{n-1}, v_h^{n-1}, \phi) \\ (i_{h,k}^n, \phi) + \frac{\delta_t}{2} a_i(i_{h,k}^n, c_{h,k}^n, u_{h,k-1}^n, v_{h,k-1}^n, \phi) = (i_h^{n-1}, \phi) - \frac{\delta_t}{2} a_i(i_h^{n-1}, c_h^{n-1}, u_h^{n-1}, v_h^{n-1}, \phi) \\ (u_{h,k}^n, \phi) + \frac{\delta_t}{2} a_u(u_{h,k}^n, u_{h,k-1}^n, c_{h,k}^n, i_{h,k}^n, \phi) = (u_h^{n-1}, \phi) - \frac{\delta_t}{2} a_u(u_h^{n-1}, u_h^{n-1}, c_h^{n-1}, i_h^{n-1}, \phi) \\ (v_{h,k}^n, \psi) + \frac{\delta_t}{2} a_v(v_{h,k}^n, c_{h,k}^n, i_{h,k}^n, u_{h,k}^n, \psi) = (v_h^{n-1}, \psi) - \frac{\delta_t}{2} a_v(v_h^{n-1}, c_h^{n-1}, i_h^{n-1}, u_h^{n-1}, \psi) \end{array} \right. \quad (5)$$

4 Numerical Simulation and Results

In this section, we investigate numerically the model introduced previously. We aim to observe the cancer response to oncolytic virotherapy via tracking the model behaviour with respect to several aspects such as: cancer cells density, tumour load ($c + i$), or cancer suppression.

For the numerical investigation, we first choose a baseline parameters (see Table 1) which are mainly based on the published studies in [29, 36, 41, 43] and present accordingly the spatial propagation of the oncolytic virus at several time stages. Second, we vary some of the parameters involved in virus dynamics and spread: the virus replication rate b , the infection rate of cancer cells ρ , and the death rate of infected cancer cells δ_i . Finally, based on the obtained results with different parameter values, we discuss the condition that can improve tumour suppression.

Visualizing the Oncolytic Viral Diffusion

In Figs. 2 and 3 we present the spatial propagation of the oncolytic virus for different relative time stages.

Table 1 Baseline parameters values for the model

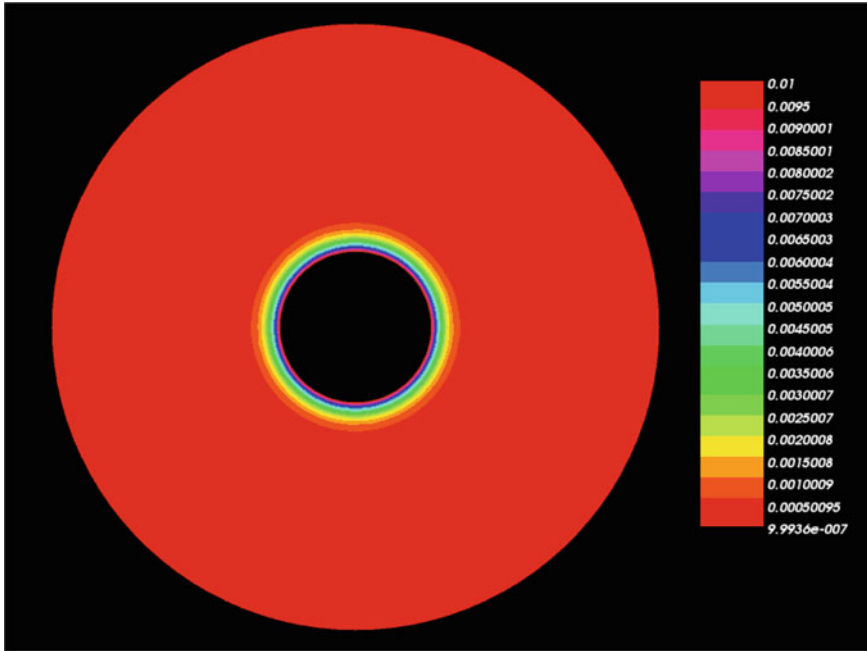
Parameter	Dimensional value	Non dimensional value	Unit	Reference
D_c (Diffusion coefficient of uninfected cancer cells)	0.00675	–	mm ² /h	[29]
D_i (Diffusion coefficient of infected cancer cells)	0.0054	–	mm ² /h	[29]
D_v (Diffusion coefficient of viruses in the reference case)	0.036	–	mm ² /h	[29]
η_c (Haptotaxis coefficient of uninfected cancer cells)	–	2.85×10^{-2}	cm ² s ⁻¹ M ⁻¹	[43]
η_i (Haptotaxis coefficient of infected cancer cells)	–	2.85×10^{-2}	cm ² s ⁻¹ M ⁻¹	[43]
μ_1 (Proliferation rate of uninfected cancer cells)	–	0.25	h ⁻¹	[43]
ρ (Infection rate of cells by viruses)	–	79×10^{-3}	mm ² /h virus	[29]
δ_i (Death rate of infected cancer cells)	0.05	–	1/h	[29]
α_c (Degradation rate of ECM by uninfected cancer cells)	–	0.15	1/h	[41]
α_i (Degradation rate of ECM by infected cancer cells)	–	0.075	1/h	[41]
μ_2 (ECM remodelling rate)	–	0.015	1/h	[41]
b (Virus replication rate)	2	–	1/h	[31]
δ_v (Clearance rate of viruses)	0.025	–	1/h	[29]
C (Carrying capacity for cancer cells and ECM)	10^6	–	Cells/mm ³	[29]
r_b (Radius of the blood vessel)	0.01	–	mm	Estimated
BVF (Blood volume fraction)	0.05	–	–	[36]
v_b (Value of v at the blood vessel)	0.01×10^6	0.01	Cells/mm ³	Estimated
c_0 (Initial condition of uninfected cancer cells)	0.5×10^6	0.5	Cells/mm ³	Estimated
i_0 (Initial condition of infected cancer cells)	0	0	Cells/mm ³	Estimated
u_0 (Initial condition of ECM)	0.5×10^6	0.5	Cells/mm ³	Estimated
v_0 (Initial condition of viruses)	0	0	Cells/mm ³	Estimated

In the following, we will discuss the outcomes of varying some parameters in the model. The main focus here is on the key parameters that are relevant to the oncolytic viruses. All the other parameter remain the same as in Table 1.

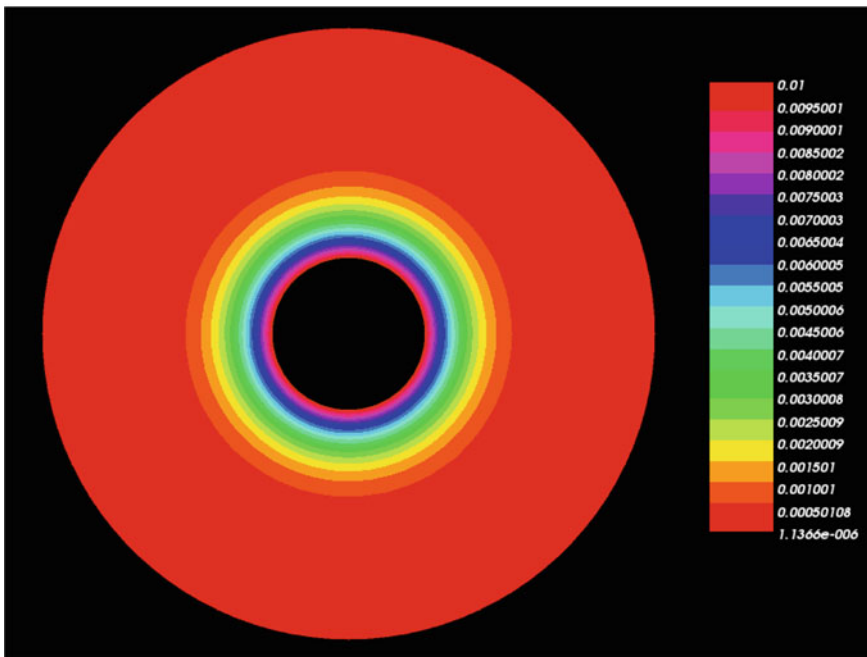
Virus Replication Rate (Burst Size) Known to be crucial within virotherapy treatment, the virus replication rate is the number of virus particles released by an infected cancer cell. We start our investigation by focusing first on the rate b at which the virus duplicate. We perform numerical experiments with $b = 0$, $b = 2$, $b = 4$, $b = 9$ and $b = 200$. Consequently, we found that there are two threshold value for the burst size. When the burst size is below the first threshold value the virotherapy always fails and the tumour grows to its maximum (carrying capacity) size (see Fig. 4). When the burst size is between the two threshold values, we obtain a partial success of the virotherapy as illustrated in Figs. 5 and 6. As an increase in the burst size will lead to a decrease in the tumour load, we can reach a minimum tumour load by genetically increasing the burst size of the virus up to the second threshold value, and still have a stable partial therapeutic success. However, once the burst size is above the second threshold, we obtain periodic oscillations with decay (Fig. 7), and if the burst size is large enough the tumour load can drop to an undetectable level then the cancer starts growing again (see Fig. 8). While the concept of oscillating tumour may seem abnormal, such behaviour have been seen in experimental observations and also in several ODE based viral dynamic models [15, 17, 23, 44, 45]. Furthermore, the oscillatory behaviour can be seen as analogous to the typical behaviour of predator-prey systems, where each population depends on the other for survival. The long period orbit can be viewed as a complete tumour eradication or tumour remission. In fact, a long period orbit can be biologically interpreted also as a complete tumour eradication: if the cancer cells population drops below certain level, this could signify extinction especially if we take into account increased clearance due to nutrient deficiency or a moderate reinforcement of virotherapy with another type of therapy. Long period orbits can also be considered as a remission or recurrence where reducing the amplitude of the orbit and increasing the period between the oscillations correspond to a more successful treatment. Furthermore, increasing exaggeratedly the burst size leads to an increase in the ECM density which will reduce the viral diffusion (see Fig. 8d).

Infection Rate of Cancer Cells In the following, we study the influence of viral infection rate (ρ) on the cancer dynamic. Experimental studies have shown that increasing the infection rate of cancer cells plays a pivotal role in the development of new anti-cancer therapies [46]. Aiming to investigate this aspect, we performed several simulation tests where we decreased and increased the baseline value $\rho = 79 \times 10^{-3}$ by a factor of three (to $\frac{\rho}{3}$ and 3ρ , respectively). As illustrated in Fig. 9 a three fold decrease in the infection rate leads to a poorer elimination of the cancer cells, compared to the case where the infection rate is increased three fold.

Death Rate of Infected Cancer Cells The death rate of infected cancer cells is the rate at which the infected cells are eliminated from the system by anti-viral

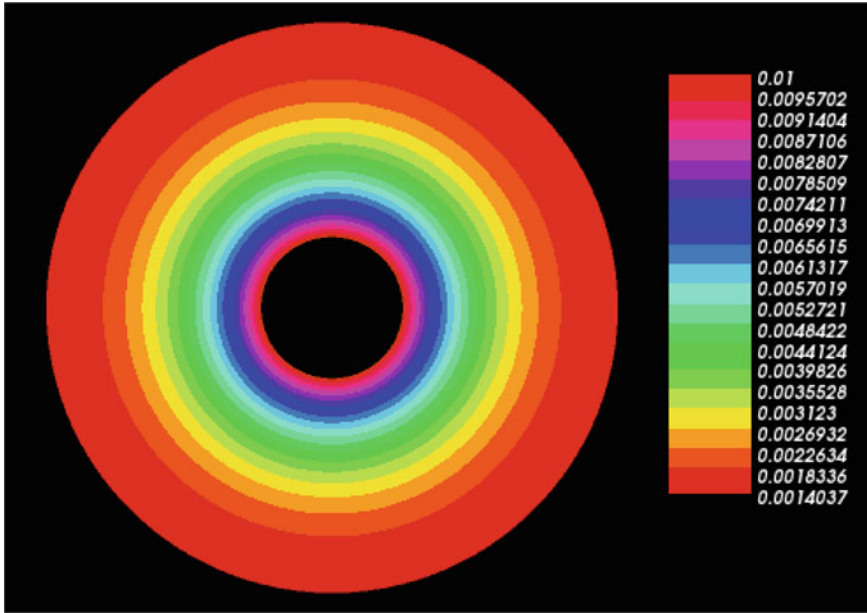


(a)

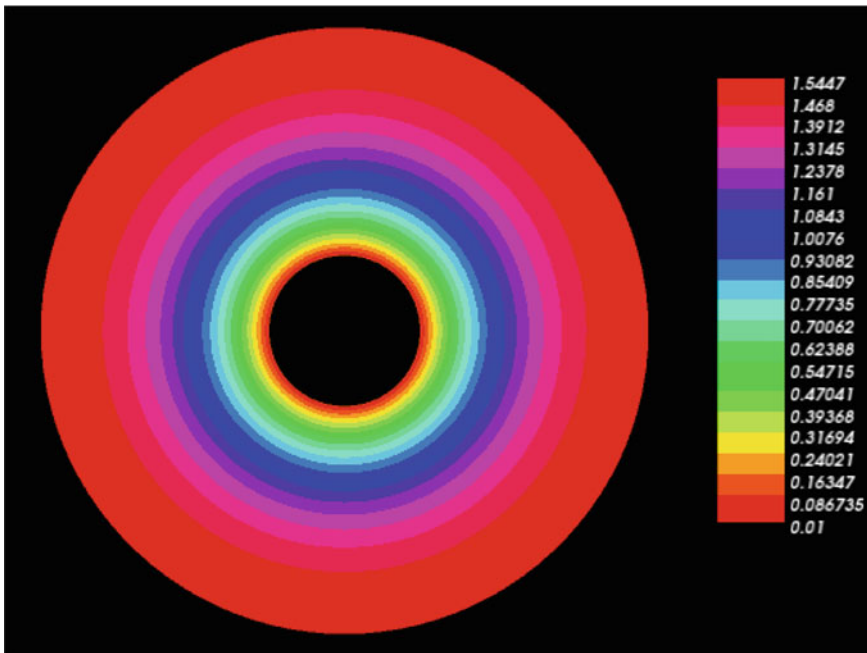


(b)

Fig. 2 Spatial propagation of the oncolytic virus for different relative time stages. (a) $t=0$. (b) $t=10$



(a)



(b)

Fig. 3 Spatial propagation of the oncolytic virus from relative time $t=100$ to $T=720$. (a) $t=100$. (b) $T=720$

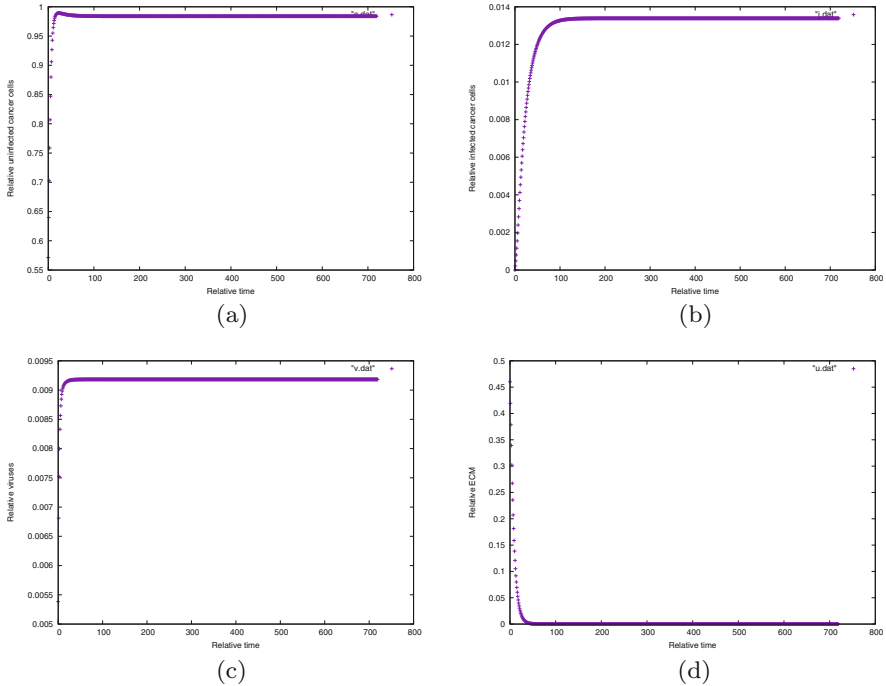


Fig. 4 Dynamics of the model at point $(0, 0.16)$ for $b = 0$. **(a)** Uninfected tumour cells. **(b)** Infected tumour cells. **(c)** Viruses. **(d)** ECM

immune response [47]. We reduce δ_i by a factor of four ($\delta_i/4$), then we notice that uninfected cancer cells are reduced dramatically (see Fig. 10d). This result is expected because the persistence of infected cancer cells promote the replication of more viruses inside these cells. Contrarily, increasing δ_i by a factor of four ($4\delta_i$) results in a weaker suppression of cancer cells as illustrated in Fig. 10a–c. However, the parameter δ_i alone does not show a clear influence towards the elimination of the tumour cells.

5 Conclusion

In this study, we introduced a system of partial differential equations coupled to an ordinary differential equation to simulate the treatment of cancer by using therapeutic viruses. The mathematical model illustrates the spatiotemporal dynamics between virotherapy, infected and uninfected cancer cells. The nonlinear terms in the coupled equations are handled semi-implicitly using an iteration of fixed-point type. The numerical simulations were carried out for different values of

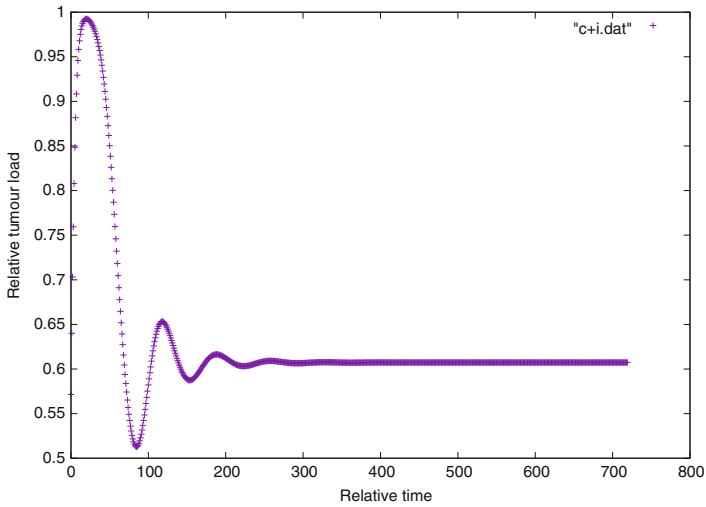


Fig. 5 Evolution of the tumour load at point $(0, 0.16)$ for $b = 2$

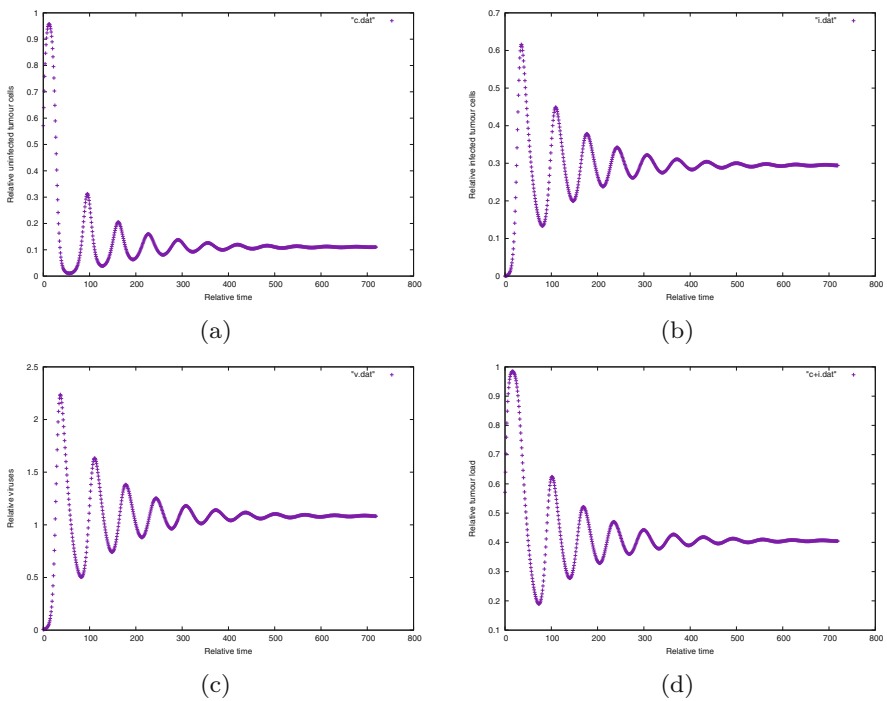


Fig. 6 Dynamics of the model at point $(0, 0.16)$ for $b = 4$. **(a)** Uninfected tumour cells. **(b)** Infected tumour cells. **(c)** Viruses. **(d)** Tumour load

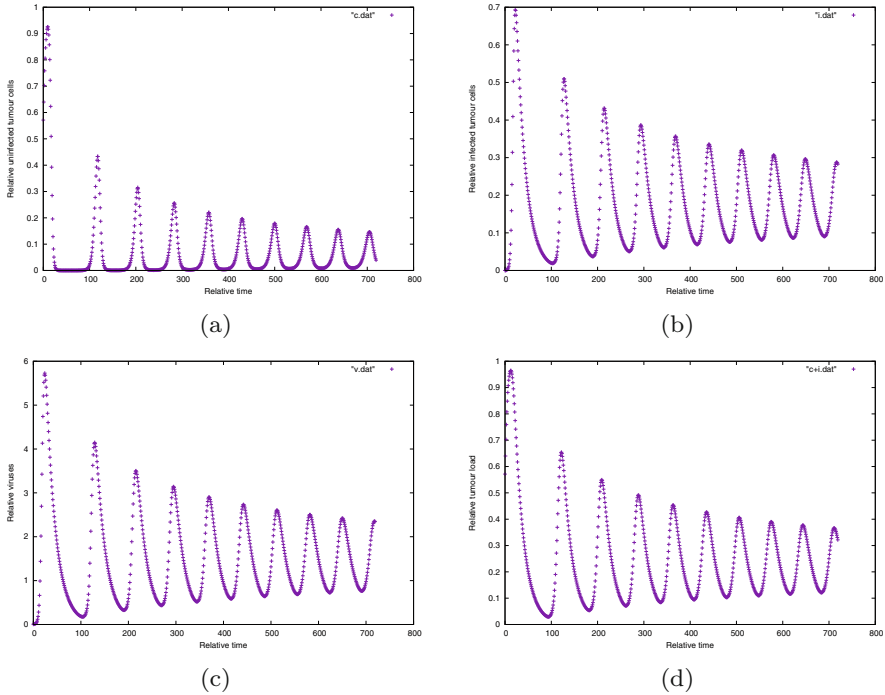


Fig. 7 Dynamics of the model at point $(0, 0.16)$ for $b = 9$. **(a)** Uninfected tumour cells. **(b)** Infected tumour cells. **(c)** Viruses. **(d)** Tumour load

the parameters related to virus dynamics and spread, namely, the burst size, the infection rate, and the clearance rate of infected cancer cells. The results showed that an improved therapy can be obtained by increasing the burst size, increasing the infection rate, and decreasing the death rate of infected cancer cells. However, since the tumour load can drop to an undetectable level then grows back, this mean that oncolytic virotherapy may not be able to eliminate all tumour cells from the body tissue. Thus, it's necessary to incorporate another treatment with virotherapy. In our study, the viruses are delivered continuously, a future research could include different delivery methods for viruses. Finally, another research point could be an investigation of the role of the immune system in the virotherapy.

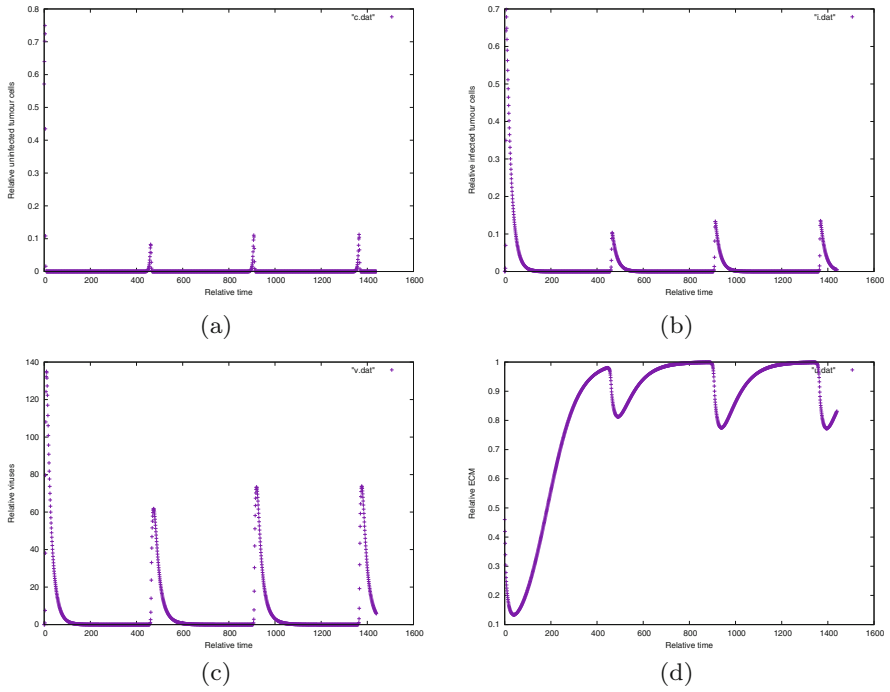
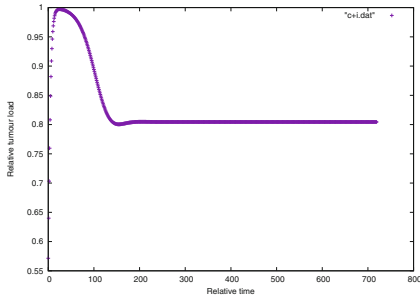
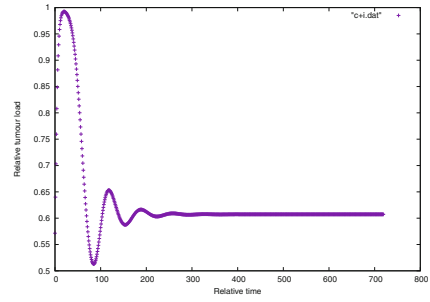


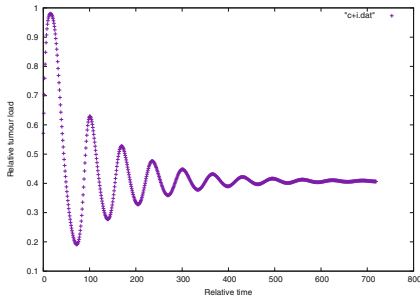
Fig. 8 Dynamics of the model at point $(0, 0.16)$ for $b = 200$. **(a)** Uninfected tumour cells. **(b)** Infected tumour cells. **(c)** Viruses. **(d)** ECM



(a)



(b)



(c)

Fig. 9 Evolution in time of the tumour load at point $(0, 0.16)$ showing two variations of the baseline viral infection rate ρ (namely: (a). Tumour load for $\frac{\rho}{5}$; (b). Tumour load for ρ ; and (c). Tumour load for 3ρ)

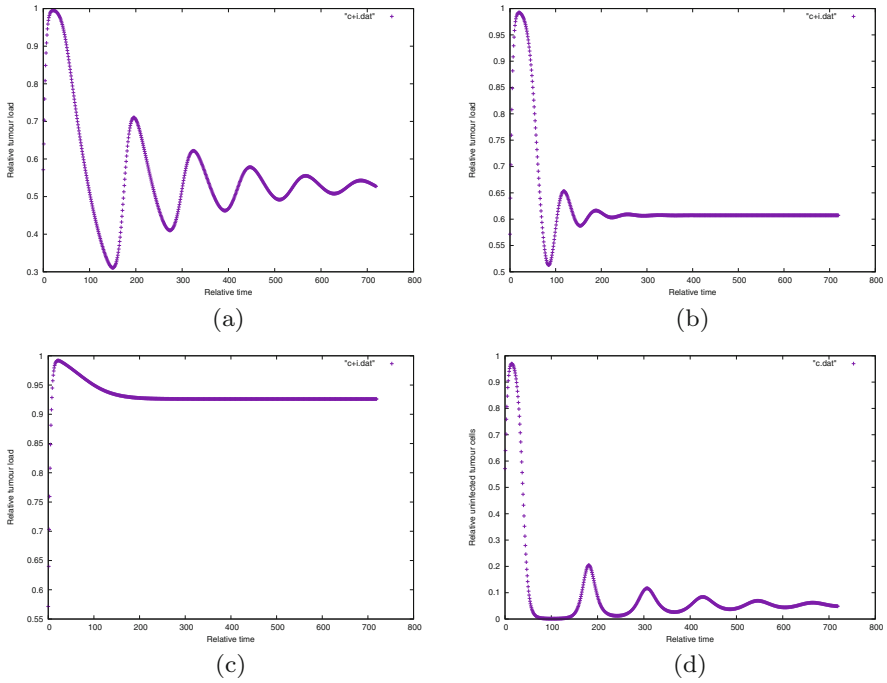


Fig. 10 Evolution in time of the tumour load at point $(0, 0.16)$ showing two variations of the baseline infected cancer cells death rate δ_i (namely: **(a)** Tumour load for $\delta_i/4$, **(b)** Tumour load for δ_i , and **(c)** Tumour load for $4\delta_i$); and **(d)** the evolution of Uninfected cancer cells for $\delta_i/4$

Reference

1. C. Fountzilias, S. Patel and D. Mhalingam, *Oncotarget* **8**, 1729 (2017).
2. H. L. Kaufman, F. J. Kohlhapp and A. Zloza, *Nat. Rev. Drug Discov* **14**, 642 (2015).
3. J. Pol, G. Kroemer and L. Galluzzi, *Oncoimmunology* **5**, e1115641 (2016).
4. S. J. Russel, K. W. Peng and J. C. Bell, *Nat. Biotechnol.* **30**, (2012).
5. A. Timalsina, J. P. Tian and J. Wang, *Bull. Math. Biol.* **79**, (2017).
6. H. Fukuhara, Y. Ino and T. Todo, *Cancer. Sci.* **107**, (2017).
7. R. Alemany, *Clinical and Translational Oncology* **15**, 182 (2013).
8. H. Wong, N. Lemoine and Y. Wang, *Viruses* **2**, 1 (2010).
9. B. Kaur, T. Cripe and E. Chiocca, *Curr Gen Ther* **9**, (2009).
10. N. Kuriyama, H. Kuriyama, C. Julin, K. Lamborn and M. Israel, *Hum Gene Ther* **11**, 1729 (2000).
11. N. Dmitrieva, L. Yu, M. Viapiano, T. Cripe, E. Chiocca, J. Glorioso and B. Kaur, *Clin. Cancer Res.* **17**, 1362 (2011).
12. D. Wodarz, *Gene Ther Mol Biol* **8**, 137 (2004).
13. D. Wodarz, *Cancer Research* **61**, 3501 (2001).
14. D. Wodarz, *Human Gene Therapy* **14**, 153 (2003).
15. N. Komarova and D. Wodarz, *Journal of Theoretical Biology* **263**, 530 (2010).
16. A. S. Novozhilov, F. S. Berezovskaya, E. V. Koonin and G. P. Karev, *Biology Direct* **1**, 1 (2006).
17. Z. Bajzer, T. Carr, K. Josic, S. G. Russel and D. Dingli, *Journal of Theoretical Biology* **252**, 109 (2008).
18. M. Biesecker, J.-H. Kimn, H. Lu, D. Dingli and Z. Bajzer, *Bulletin of Mathematical Biology* **vol. 72**, 469 (2010).
19. A. Friedman, P. Tian, G. Fulci, A. Chiocca and J. Wang, *Cancer Research* **Vol 66**, 2314 (2006).
20. P. Tian, *Mathematical Biosciences and Engineering* **Vol 8**, 841 (2011).
21. A. E.-A. Laaroussi, M. E. Hia, M. Rachik, E. Benlahmar and Z. Rachik, *Applied Mathematical Sciences* **8**, 929 (2014).
22. P. S. Kim, j. j. Crivelli, I.-K. Choi, C.-O. Yun and J. R. Wares, *Mathematical Biosciences and Engineering* **12**, 841 (2015).
23. D. Dingli, C. Offord, R. Myers, K.-W. Peng, T. Carr, K. Josic, S. Russell and Z. Bajzer, *Cancer Gene Therapy* **16**, 873 (2009).
24. M. A. Nowak and R. M. May, *Oxford University Press*, (2000).
25. C. Alvarez-Breckenridge, B. Choi, C. Suryadevara and E. Chiocca, *Curr. Opin. Virol.* **13**, 25 (2015).
26. M. A. Nowak, C. R. M. Bangham, *Science* **272**, 74 (1996). **2**, 131 (2011).
27. J. T. Wu, H. M. Byrne, D. H. Kirn and L. M. Wein, *Bulletin of Mathematical Biology* **vol. 63**, 731 (2001).
28. L. M. Wein, J. T. Wu and D. H. Kirn, *Cancer Research* **vol. 63**, 1371 (2003).
29. B. I. Camara, H. Mokrani and E. Afenya, *Mathematical Biosciences and Engineering* **10**, 565 (2013).
30. J. Malinzi, P. Sibanda and H. Mambili-Mamboundou, *Mathematical Biosciences* **263**, 102 (2015).
31. J. Malinzi, A. Eladdadi and P. Sibanda, *J. Biological Dynamics* **11**, 244 (2017).
32. J. Malinzi, R. Ouifki, A. Eladdadi, D. F. M. Torres and K. A. J. White, *Math. Biosci. Eng.* **15**, 1435 (2018).
33. S. B. Carter, *Nature* **213**, 256 (1967).
34. A. S. G. Curtis, *Journal of Embryology and Experimental Morphology* **22**, 305 (1969).
35. J. Pascal, E. L. Bearer, Z. Wang, E. J. Koay, S. A. Curley and V. Cristini, *Proceeding of the National Academy of Sciences* **vol. 110**, 14266 (2013).
36. Z. Wang, R. Kerketta, Y. L. Chuang, *PLoS Computational Biology* **vol. 12**, e1004969 (2016).
37. K. T. Nguyen, *Journal of Nanomedicine & Nanotechnology* **vol. 2**, (2011).
38. A. Laird, *J. Cancer* **18**, 490 (1964).

39. C. Guiot, P. Degiorgis, P. Delsanto, P. Gabriele and T. Diesboeck, *Journal of Theoretical Biology* **225**, 147 (2003).
40. T. Cox and J. Erler, *Dis. Model Mech* **4**, 165 (2011).
41. M. A. J. Chaplain and G. Lolas, *Netw. Heterog. Media* **1**, 399 (2006).
42. S. Ganesan and L. Tobiska, *Internat. J. Numer. Methods Fluids* **57**, 119 (2008).
43. L. Peng, D. Trucu, P. Lin, A. Thompson and M. A. J. Chaplain, *Bulletin of Mathematical Biology* **79**, 389 (2017).
44. L. R. Paiva, C. Binny, S. C. Ferreira and M. L. Martins, *Cancer Research* **vol. 69**, 1205 (2009).
45. M. I. Titze, J. Frank, M. Ehrhardt, S. Smola, N. Graf and T. Lehr, *European Journal of Pharmaceutical Sciences* **vol. 97**, 38 (2017).
46. J. Maroun, M. M. Noz Alia, A. Ammayappan, A. Schulz, K. W. Peng and S. Russel, *Future Medicine* **12**, 193 (2017).
47. A. Filley and M. Dey, *Frontiers in Oncology* **106**, 8 (2017).